The reconstructed images, AP, SNR and Time comparisons are shown in Figs. 2 and 3 respectively. The results show that CG provides better results than POCS, even at higher AF but the time noted for POCS is much lesser than the CG because of its precise algorithm and lesser computations.

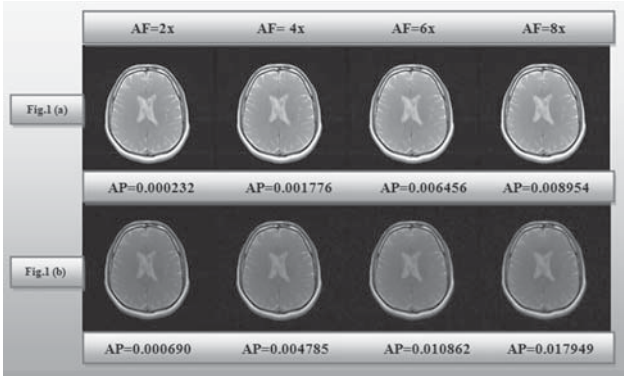


**Fig. 2** Results of Compressed Sensing applied on human brain image. **a** Image reconstructed using CG algorithm. **b** Image reconstructed using POCS algorithm

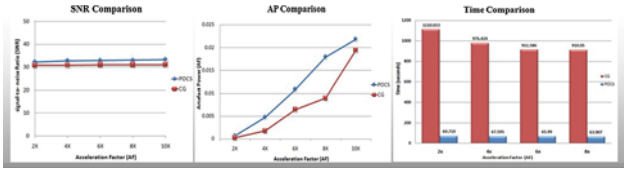


**Fig. 3** Graphical illustration using the results of CG and POCS compared with respect to signal-to-noise Ratio (SNR), Artifact Power (AP) and Time span required for 15 iterations at increasing Acceleration Factors (AF)

**Discussion/Conclusion:** We conclude that CG provides better results for compressed sensing but as we need fast image reconstructions in CS, POCS may be a good choice providing slightly compromised image quality in significantly lesser time.

**References:**

[1] Lustig, M et al., Magnetic resonance in medicine, 2007.
[2] Alexei A. Samsonov et al., Medical Imaging, 2003.
[3] Kai Tobias Block et al., Magnetic Resonance in Medicine, 2007.
[4] Mariya Doneva et al., Compressed Sensing (CS) Workshop, 2011.
[5] David O. Walsh, et al., Magnetic Resonance in Medicine.
[6] Philip M. Robson et al., Magnetic Resonance in Medicine, 2008.

## 412
## Evaluation of image-based bias field correction at 7 T

**M.J. Van Rijssel**[1], J.P.W. Pluim[2], B.H.M. Van Der Velden[2], T.A. Van Der Velden[3], E. Krikken[3], J.P. Wijnen[3], K.G.A. Gilhuijs[2], D.W. Klomp[3]
[1]*Radiology, University Medical Center Utrecht, Utrecht/NETHERLANDS,* [2]*Image Sciences Institute, University Medical Center Utrecht, Utrecht/NETHERLANDS,* [3]*Radiology, UMC Utrecht, Utrecht/NETHERLANDS*

**Purpose/Introduction:** $B_1$ non-uniformities lead to intensity variations in MR images, which are often compensated for by fitting a smooth multiplicative field to the affected image [1]. We investigated this method's ability to account for local $B_1$ differences in $T_1$-weighted 7 T breast images containing a large spread of $T_1$ values such as DCE-MRI, using acquired $B_1$ maps.

**Subjects and Methods:** Three-dimensional $B_1$ maps (Actual Flip-angle Imaging [2]) and $T_1$-weighted bilateral breast MRI ($\theta_{nom} = 8°$, TR = 7 ms) were obtained from 10 healthy female volunteers (27 ± 5 years) using a 4-channel transceiver.

The reference $B_1$-based bias field was calculated using the steady-state signal expression:

$$SI(\theta) = \Lambda \frac{1 - e^{-TR/T_1}}{1 - e^{-TR/T_1}\cos(\theta)} \sin(\theta) B_1^-, \quad \text{where } \theta = \theta_{nom} B_1^+$$

In reconstruction, we defined fixed amplitude and phase between all 4 channels (identical to transmit) and considering the relatively long wavelength of RF-fields in lipid rich breasts it was assumed that $B_1^- \approx B_1^+$. The reference bias field was calculated using either $T_1 = 540$ ms (e.g. lipids) and 54 ms (e.g. gadolinium enriched tissues) for the entire image. The image-based bias field algorithm (N4 [1]) was applied twice: first a single pass with a coarse grid that has smallest spacing in the A–P direction, then a multiscale approach using an isotropic grid. The reference ($B_1$-based) and the image-based (N4) bias fields were each applied to the $T_1$-weighted images. Masks were applied to exclude areas where the image-based or the reference bias field was not known. The ratio between the reference and the image-based bias fields was calculated as: R = reference bias/image-based bias.

**Results:** Three volunteers were excluded due to unreliably low signal during $B_1$ mapping. Figure 1 shows an example of a $T_1$-weighted breast image (left), corrected with the image-based bias field (middle), and the reference bias field for fatty tissue (right).

Figure 2 shows the distribution of bias estimation ratios for both $T_1$ values in included volunteers; the Table 1 shows distribution statistics per volunteer.

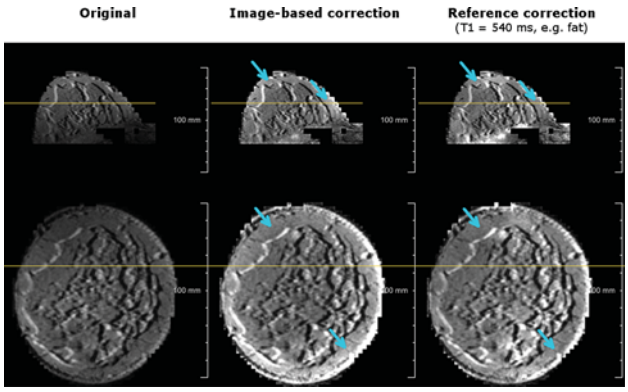


**Fig. 1** Example showing that the image-based (N4) correction method changes the local, endogenous contrast of fatty vs fibroglandular tissue when compared to the reference correction for fat (*arrows*). *Yellow line* indicates slice position in the other orientation

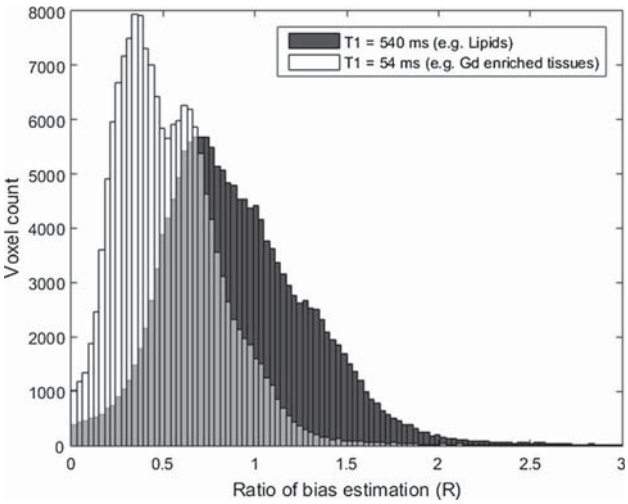


**Fig. 2** Ratio distribution of reference bias over image-based bias for two tissue types calculated with T1 = 540 ms (e.g. lipids, *black*) and T1 = 54 ms (e.g. gadolinium enriched tissues, *white*)

**Table 1** Ratio (R) statistics per volunteer

| Volunteer | 1 | 4 | 6 | 7 | 8 | 9 | 10 | Summary |
|---|---|---|---|---|---|---|---|---|
| **T1 = 540 ms** | | | | | | | | (Geom.mean ± SD) |
| Geometric mean | 0.96 | 0.99 | 0.76 | 0.74 | 0.75 | 0.75 | 0.77 | **0.81 ± 0.11** |
| FWHM | 0.32 | 0.52 | 0.43 | 0.59 | 0.38 | 0.45 | 0.61 | **0.47 ± 0.11** |
| **T1 = 54 ms** | | | | | | | | |
| Geometric mean | 0.48 | 0.56 | 0.45 | 0.46 | 0.37 | 0.38 | 0.50 | **0.45 ± 0.07** |
| FWHM | 0.47 | 0.84 | 0.49 | 0.66 | 0.20 | 0.28 | 0.48 | **0.49 ± 0.22** |

**Discussion/Conclusion:** $B_1$ mapping allows evaluation of bias field correction methods. We demonstrated a substantial deviation (54 % on average, $\varepsilon = 1 - R$) in contrast-enhanced tissues in $T_1$-weighted breast MRI at 7 T even after image-based bias field correction. As inferred for this N4 implementation, incorporation of $B_1^+$ and $B_1^-$ maps remains essential in quantified DCE-MRI.

**References:**

[1] Tustison et al., IEEE Trans. Med. Imag., 2010. 29(6):1310–1320.
[2] Yarnykh, MRM, 2007.57(1):192–200.

## 413

## Noise reduction in cardiac cine images using temporal filtering and noise estimation

**K. Isogawa**[1], T. Ono[1], T. Takeguchi[1], N. Matsumoto[1], N. Ichinose[2], H. Takai[2]

[1]*Corporate Researcy & Development Center, Toshiba Corporation, Kawasaki/JAPAN,* [2]*MRI Systems Division, Toshiba Medical Systems Corporation, Otawara/JAPAN*

**Purpose/Introduction:** The variance of noise differs across pixels in an image as well as across images. To avoid oversmoothing, noise reduction (NR)[1] strength should be reduced for pixels with small variance of noise. Low-noise pixels can be specified using the coil sensitivity, but the variance of noise of the pixels remains unknown. Additionally, noise estimation methods[2] require a still image with homogeneous S/N across pixels. We propose an NR strength control method with cine images used to handle the inhomogeneous S/N across pixels.

**Subjects and Methods:** Retrospective ECG-gated 2D steady-state free precession cardiac cine images (Fig. 1) were acquired using a 1.5-T MRI scanner with an 8-ch PI coil. The scanning conditions were pixel bandwidth = 977 Hz, TR/TE = 4.2/2.1, flip angle = 65°, slice thickness = 8 mm, pixel spacing = 0.86 × 0.86 mm, matrix = 240 × 192, reduction factor = 1.5, number of phases = 20.

First, the coil sensitivity and geometric factors are converted to an S/N map (Fig. 2). Second, assuming constant S/N, the temporal average and variance of the signals of each pixel are calculated and then corrected using the S/N map. Corrected data from the entire image is used to estimate the Rician distribution parameters to avoid overestimation of variance caused by cardiac motion because the heart is sufficiently small in cine images. Then, the estimated Rician distribution and S/N map are used to estimate the variance of noise for each pixel. The estimated variance is proportional to NR strength (Fig. 3) for a temporal nonlinear NR filter.

**Results:** NR strength in higher S/N region A (Fig. 1) is set lower than in noisy region B (Fig. 1). Oversmoothing of the temporal profile of high-S/N pixels (Fig. 4) is avoided. Simultaneously, the profile of low-S/N pixels is smoothed (Fig. 5). The texture of the cardiac valve in A is maintained (Fig. 6c), while noise in B is reduced (Fig. 6g).


**Fig. 1** Input

**Fig. 2** S/N Map